Distribution Agreement

In presenting this thesis or dissertation as a partial fulfillment of the requirements for an advanced degree from Emory University, I hereby grant to Emory University and its agents the non-exclusive license to archive, make accessible, and display my thesis or dissertation in whole or in part in all forms of media, now or hereafter known, including display on the world wide web. I understand that I may select some access restrictions as part of the online submission of this thesis or dissertation. I retain all ownership rights to the copyright of the thesis or dissertation. I also retain the right to use in future works (such as articles or books) all or part of this thesis or dissertation.

Signature:

_____ _____

Jiaqi Zheng Date

Growing length scale near the jamming point in a low-friction, continuously sheared granular system

By

Jiaqi Zheng

Master of Science

Physics

_____

Justin Burton
Advisor

_____

Stephan Boettcher
Committee Member

_____

Connie Roth
Committee Member

_____

Eilaf Egap
Committee Member

Accepted:

_____

Lisa A. Tedesco, Ph.D.

Dean of the James T. Laney School of Graduate Studies

_____

Date

Growing length scale near the jamming point in a low-friction, continuously sheared granular system

By

Jiaqi Zheng
B.Sc., Shandong University, 2014

Advisor: Justin Burton, PhD

An abstract of
A thesis submitted to the Faculty of the
James T. Laney School of Graduate Studies of Emory University
in partial fulfillment of the requirements for the degree of
Master of Science
in Physics
2016

Abstract

Growing length scale near the jamming point in a low-friction, continuously sheared granular system
By Jiaqi Zheng

Granular materials are the second largest amount of material used in industry other than water. One of their interesting properties is that they can change between a flowing state to a rigid state, which is called a jamming transition. In the jammed state many macroscopic observables exhibit critical behavior and a diverging length scale at the jamming point. Many studies of the details of the jamming transition are simulations conducted in a static and frictionless system. Direct experimental evidence of critical behavior is hard to find partially because correlation lengths are difficult to visualize and depend on the system properties. Moreover, in experimental granular studies, friction is very hard to minimize. In order to experimentally study the critical behavior of the jamming transition, we built a low-frictional 2D granular system with a controllable density. By tracking the particles' movement in the system, we observed a growing length scale in the system dynamics. We defined a cluster of spheres which collectively moved like a rigid body. We found that the size of this cluster quickly grows after the system has jammed, and eventually reaches the boundaries of the system.

.

Growing length scale near the jamming point in a low-friction, continuously sheared granular system

By

Jiaqi Zheng
B.Sc., Shandong University, 2014

Advisor: Justin Burton, PhD

A thesis submitted to the Faculty of the
James T. Laney School of Graduate Studies of Emory University
in partial fulfillment of the requirements for the degree of
Master of Science
in Physics
2016

Acknowledgements

Without the invaluable support, guidance, and knowledge provided by my excellent advisor Dr. Justin Burton, I certainly would not have reached this point in my studies. I thank him for giving so much advice of my research and study. It has been a great experience in my life to do research and study in his lab. I admire his enthusiasm for science and teaching. I also want to thank Dr. Roth, Dr. Boettcher and Dr. Egap for being my committee members and gave me support and help. In addition, I want to thank Rui Wu for initiating the project and Dominic Robe for helping me with data analysis; their contributions were very important to this project.

I also want to thank Clay Wood for being supportive and helpful in my life. He helped me through a lot of difficulties of living in a different county. I also want to thank my friend Daniel Hanfelt and Brian Zhao for giving my advice for writing, my coworkers Xiaolei Ma, Justin Pye, Stephen Frazier, Nicholas Cuccia, and Janna Lowensohn for giving me help in lab and all my friends in the Emory physics department for your support. Finally, I want to thank my parents for all their effort put in raising and educating me.

Table of Contents

List of graphs

baseline force data for systems where spheres remain in the quasi-2D layer.

13. Fig.13 (a) A picture of the system while shearing. This corresponds to the 7th data point for the shear force. (b) A zoomed-in picture for (a) at a small region with a sphere popping out of the plane.
14. Fig.18 The original gray scale image and the binary image.
15. Fig. 15 (a) Pixel density vs. compression distance. (b) Change in the force on the movable wall in response to compression to the movement of the wall (same as Fig.12 (b)).
16. Fig.16 Force sensors' data with and without shearing for six different packing system (same data as shown in Fig. 12(b) and Fig. 15 (b))
17. Fig.17 The averaged pixel density changing in y direction (normalized by d_0 average particle diameter) in six different packing fractions over 1000 seconds
18. Fig.18 Trajectories of spheres in systems with six different density over 200 seconds start from t=100s. The packing fraction for the six data set are (a) $\phi = 0.781$, (b) $\phi = 0.785$, (c) $\phi = 0.787$, (d) $\phi = 0.790$, (e) $\phi = 0.793$, (f) $\phi = 0.796$. The x and y axis are normalized by averaged particle diameter d_0.
19. Fig.19 distribution of the displacement over 1000 seconds of systems with six different packing fractions.
20. Fig.20 Average velocity for 100 seconds vs. y normalized by mean particle diameter.
21. Fig.21 Displacement of 100 seconds for system with density (a) 0.787 (compression 6.35mm, third data point with shearing) and (b) 0.793 (compression 12.7mm, the fifth data point with shearing)

22. Fig.22 (a) The center of the collected movement of cluster in different threshold and packing fraction; (b) Projection of (a) on packing fraction and center position plane showing.

23. Fig.23 A more complete version of jamming diagram with intermittent states and with an indication of position of the ϕ_x . SJ is the shear jamming state and F is the fragile state discover by Dapeng Bi [7]. ϕ_J is the jamming point; ϕ_s is the shear jamming point.

Chapter 1

Introduction

Granular material is pervasive in our life. Examples include sugar, flour, coffee and snow. In industry, granular materials are widely used: coal is one of the major sources of energy, sand is used in building dams and beaches, and powdered and grained metals and plastics are used in making all kinds of living necessities like containers and furniture. Scientists have been devoted to studying granular materials for more than two centuries [1-4]. One of the special characteristics of granular materials is that, unlike normal liquid material which can flow and solid material which is rigid, granular material can sometimes flow and is sometimes rigid. For example, a sand pile is seemingly rigid on a floor, but when the angle of the floor is tilted to a certain degree the sand pile will start an avalanche flow. So, controlling the state of granular material is a very important in both daily life and industry.

There are a lot of factors that affect the state of granular material. In 1998, A. J. Liu and S. R. Nagel developed a jamming diagram depicting the transition of amorphous materials from a flowing to a rigid state [5]. The diagram (Fig. 1) combines three important properties which describe the state of amorphous materials: temperature, density, and applied load. For the granular systems composed of macroscopic particles, thermal motion is extremely low, so temperature is not a factor that will affect its state. Typically, only the density and shear load are important for granular materials.

The interesting thing about the jamming transition is that it shares similarities with both first-order and second-order phase transitions, i.e. it shows both discontinuities and power-law scaling at the critical point. Given these similarities, we may expect there to be a diverging correlation length at the transition. There are a few types of length scales that have been discussed in the literature. Two of them are related to the properties of static systems [10-12]. Another length scale comes from measurements of velocity correlations in sheared granular systems [13]. However, these measurements have mostly been limited to simulations, and direct experimental evidence is rare. Moreover, most of the simulations focus on frictionless system which also makes results difficult to be verified in experiment.

To address these issues, we built a low-friction 2D granular system composed of hydrogel particles floating on a layer of heavy oil. In the experiment, we can apply continuous shear to the system and we can control the density of the granular system by changing the volume of the tank in which the particles are sitting. By tracking particle movement and measuring the force that the particles apply on the side walls of the system, we found that shearing the system induces motion of the particles over a growing length scale. This length scale saturates at the size of the system when the packing fraction is a few percent larger than the critical packing fraction where the system initially jams. Our results suggest that coherent motion in jammed systems isn't simply defined by the distance to the jamming point, and may require significantly larger

densities.

1.1 Jamming diagram

Granular material is a type of amorphous material. It is a conglomeration of discrete, solid, macroscopic particles. However, amorphous material is a very broad category which includes foams, glasses or other complex fluids. Amorphous material can change between a liquid-like state and a rigid state which is very different from the formation of crystalline solids (freezing). A crystal can change from a flowing liquid to a solid, highly-ordered atomic structure at a specific temperature. For amorphous material, the transition does not happen immediately over the whole material, and the structure is disordered. This transition is called the jamming transition.

The jamming transition is affected by many factors. A. J. Liu and S. R. Nagel in 1998 [5] showed a phase diagram suggesting that all amorphous materials share the same generic behavior. They suggested that temperature, shear stress and density are important variables which affect jamming [5-7]. In this diagram (Fig. 1), the jammed region is defined near the origin, at low temperature, low stress, and high density. One special point in the diagram is called point J. It is located on the inverse density axis where shear load and temperature are zero. As the shear load or the temperature increases, the material can unjam through thermal fluctuations or external forcing. At zero temperature and stress, the material will jam by changing the density, the average number of contacts per particle changes drastically, and the shear modulus, bulk modulus, and the pressure

change in a power-law fashion with the system's packing fraction φ (density) [6].

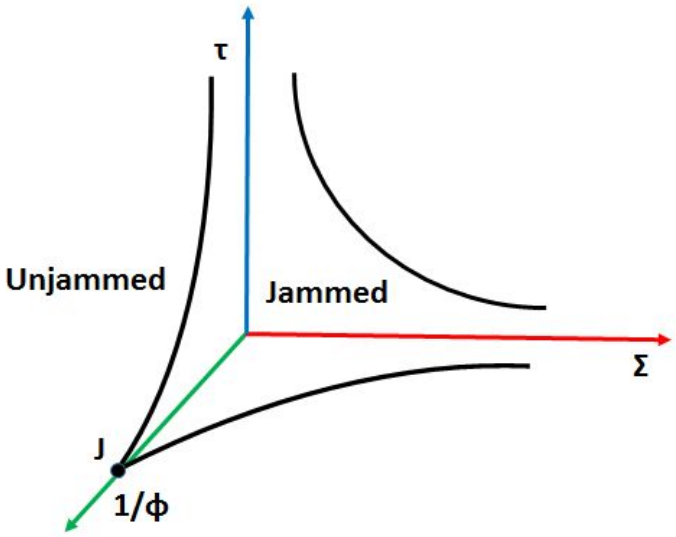

Fig.1 Jamming phase diagram, first introduced in reference [5]. As value of the inverse density, shear stress, and the temperature varying, the amorphous materials can change from unjammed to jammed states.

Many kinds of materials can be described in the diagram: colloidal suspensions, like milk, chocolate and mayonnaise, become colloidal glasses as the density is increased near point J. Beyond a certain concentration, a colloidal suspension is said to be a colloidal glass; the system resembles a liquid, yet motions within the suspension are slow enough that it can be considered essentially frozen. Foams become rigid as the shear load is decreased below the yield stress, and viscous liquids freeze solid when gradually cooled, a process which can be described in the temperature vs. density plane [14]. Among those, granular materials, which are usually considered as having little thermal energy, are usually put in the shear load vs. $1/\varphi$.

1.2 Length scale at jamming for static granular system

It has been known since the early 2000's that there are diverging length scales associated with the jamming transition [6, 15]. One early seminal paper which identifies a diverging length scale in static granular systems refers to the cutting length which focuses on Z (the average number of overlaps a particle has with its neighbors) [10]. For a frictionless system in the unjammed region, the number of the overlap particles is $Z=0$. If the packing fraction is low, particles can have no contact with other particles and have a lot of empty space around them, thus can easily rearrange. As the packing fraction increases to the jamming point, the system is rigid and Z jumps to a critical value $Z^C = 2d$, with d representing the dimension of the system. This is because of Maxwell's criterion for rigidity, which states that the number of interparticle forces $NZ/2$ (N is the number of particles; the factor ½ is due to the fact that each contact is shared by 2 particles) must be at least the number of degree of freedom, which is Nd. So, we get $Z^C = 2d$ [6, 17-19]. Z^C gives a minimum value for a cluster of granular particles to be rigid. To determine the length scale of a rigid cluster, we can imagine a chunk of material of size l is cut from the d-dimensional system. The number of contacts missing at the boundary is proportional to l^{d-1}. When it is cut out, a number of the contacts, $c_1 l^{d-1}$, are broken at the perimeter. The excess number of contacts in the bulk is $c_2(Z - Z^C)l^d$, which is the difference between actual number of contacts and the critical number of contacts in the bulk. c_1 and c_2 are constants depending on the shape the cluster. The

difference between the number of missing contacts at the perimeter and the excess number of contacts in the bulk is $c_1 l^{d-1} - c_2(Z - Z^C) l^d$. For the cluster to be rigid this difference must be larger than 0. At the limit when this difference is 0, the length $l^* \sim (Z - Z^C)^{-1}$, where l^* is the critical length for the cluster to be rigid [10]. So, for a cluster of granular particles to be rigid the size of the cluster must be larger than the l^*.

Clear simulation results have already shown evidence of diverging length scales in static granular systems. One early observation in simulations of two-dimensional granular systems was conducted by Wouter G. Ellenbroek in 2006 [16]. In their simulation, they varied the value of *Z* by adding a single grain one by one each time and found that the scale of the force response over the system diverging as the system approaches jamming transition. They quantified the force response by measuring RMS fluctuations of the changes in interparticle forces at a specified radius *r*. In their results, the relative fluctuation (fluctuation divided by average value of contact force) is a constant when $r\Delta Z \simeq 6$. This constant mark a place where the fluctuation stops growing with a critical length $l^* \sim 6/\Delta Z$. This is an evidence of the diverging length scale behavior $l^* \sim (Z - Z^C)^{-1}$. Another recent simulation found a clearer and direct observation of a diverging length scale at the jamming transition [11]. This study focuses on the "rigidity length", which is related to the size of a cluster of particles that have a sufficient number of contacts to hold the whole cluster stable. The rigidity length of the cluster is defined as the radius of gyration of the cluster. The simulation results shows

that the rigid length diverges at $l \sim (Z - 2d)^{-1}$

Experimental efforts have also been made to look for diverging length scales. One distinction in the experiments is that the packing fraction is usually used instead of *Z*, because *Z* is a microscopic value. However, it is also related to packing fraction as a macroscopic value and packing fraction is very convenient to measure in experiment. According to numerous simulations, the $Z - Z^{C} \sim \Delta\phi^{0.5}$ [6, 7, 20], where $\Delta\phi$ is the difference between packing fraction and critical packing fraction at point J. One recent experiment aimed to find characteristic length scales in static granular materials using tapioca spheres made of starch [21]. The particles can swell in water from dry particles, which is a slow process, taking approximately 24 hours to fully swell. During the experiments, the authors imaged the system while it swelled, which changed the packing fraction, and they tracked the particles' movements. By analyzing the displacement field, they extracted a static length scale, the correlation length, from the cluster structure. The results shows that the correlation length grows as the packing fraction increases from unjammed to jamming point and diverges at the jamming point.

1.3 Sheared granular system and diverging length scales

Granular systems are considered athermal because the cost of energy to move one particle is many orders of magnitude larger than the thermal energy of each particle. So, external excitement to introduce particle movement, like shearing, is usually needed in

the study of the dynamics of granular materials. Even though thermal effects are not considered here, the system's dynamics are still very complex, like the dilatancy, arching and segregation effects [22-26]. We are interested in identifying characteristic dynamical length scales near the jamming point. So, how does shearing affect the jamming? It turns out that shearing will induce some modified jamming states which makes the original jamming diagram a little different.

These shear jamming states were originally discovered in an experimental study conducted by Bi Dapeng et al. [27]. In the shear jamming states, whether or not a system is jammed depends on their history. In their experiments, they used photoelastic disks to build a two-dimensional system which can show force chains. The way they determined jamming is to see whether or not the force chains percolated throughout the system in all directions. What they found is that some states, which were initially unjammed, developed force chains which percolated in both the x and y-direction after shearing the system and returning it to the original state. This altered the original jamming diagram by adding some regions with extra intermittent states. Because jamming is different when shearing, the length scales may also be different in a dynamic granular system.

There are some studies that indicate there is some growing length scales in a dynamic systems. For example, in one simulations, a quasi-static shear flow is applied to a 2d frictionless, granular system by the Lees–Edwards boundary condition [13]. The author calculated the displacement correlation $G(y)$ in y (along shear direction) and used

the *y* value at the lowest point of *G(y)* to be a length scale. The result showed that this length scale $\zeta(\varphi)$ diverges at jamming point $\varphi_c = 0.84$ with a correlation length exponent in the range of *0.8 - 1.0*. However, there is no experimental study that attempts to characterize a diverging length scale in dynamic granular systems.

1.4 Low friction experiment

In order to find characteristic length scales associated with motion in a dynamic granular system, we first look into the difference between the simulation work and experimental work. One of the major differences between them is friction [21, 27, 28]. One way to intuitively think about how friction can affect the length scale is by the number of contacts per particle *Z*. As we know from Chap. 1.2, the growing length scales in static systems are related to *Z*. However, a frictional system requires smaller *Z* for the system to be rigid. If the spheres have static friction, the tangential friction forces introduce torque balance conditions for a stable system, which changes the counting of the number of degrees of freedom. The result is that *Z* required to make the system rigid is $Z = d - 1$, not $2d$; this will make the scaling relationship different [29]. There are also simulation results showing the difference between frictional and frictionless system. For example, Michio Otsuki and Hisao Hayakawa in 2011 found varying pressure responses to systems under shear with different friction coefficients [30].

Experimental studies with low-friction particles will be very helpful for understanding amorphous materials. This will help make a connection between numerous

theoretical studies and experiments. Some scientists have already tried to experimentally study shear jamming without basal friction [28]. However, it is very difficult to eliminate inter-particle friction. In our experiment, we have built a very low-friction granular system by: 1) using hydrogel particles composed mostly of water and 2) making the spheres float on an oil layer to reduce the basal friction. We found a length scale of rigid body movement grows as the packing fraction changes. This length scale grows rapidly at the jamming point and reaches the system size at a packing fraction higher than the jamming point.

1.5 Thesis outline

This thesis consists of 5 chapters detailing the work completed in the pursuit of a Master of Science degree at Emory University.

- Chapter 2 discusses the experimental setup in detail, including the outline of all parts of the experimental system and details about how the system was constructed.
- Chapter 3 describes the methods of data acquisition from the force sensors (when shearing the system and when the system is relaxed) and recording images of the system for analysis (particle tracking).
- Chapter 4 is the analysis and results.
- Chapter 5 is the conclusion, discussion, and future directions of this project.

Chapter 2

Experimental approach

2.1 Outline of the experimental setup

The system consists of five parts: a quasi-2D layer of hydrogel spheres; a movable wall (which has force sensors on it); a shearing belt controlled by the power supply; an imaging system with a high resolution camera, a LED panel under the particles, and a pump and draining system which can adjust the water level. A photo of the whole system setup is shown in Fig. 2 and a diagram of the system is shown in Fig. 3.

Fig.2 The photo for the entire set-up.

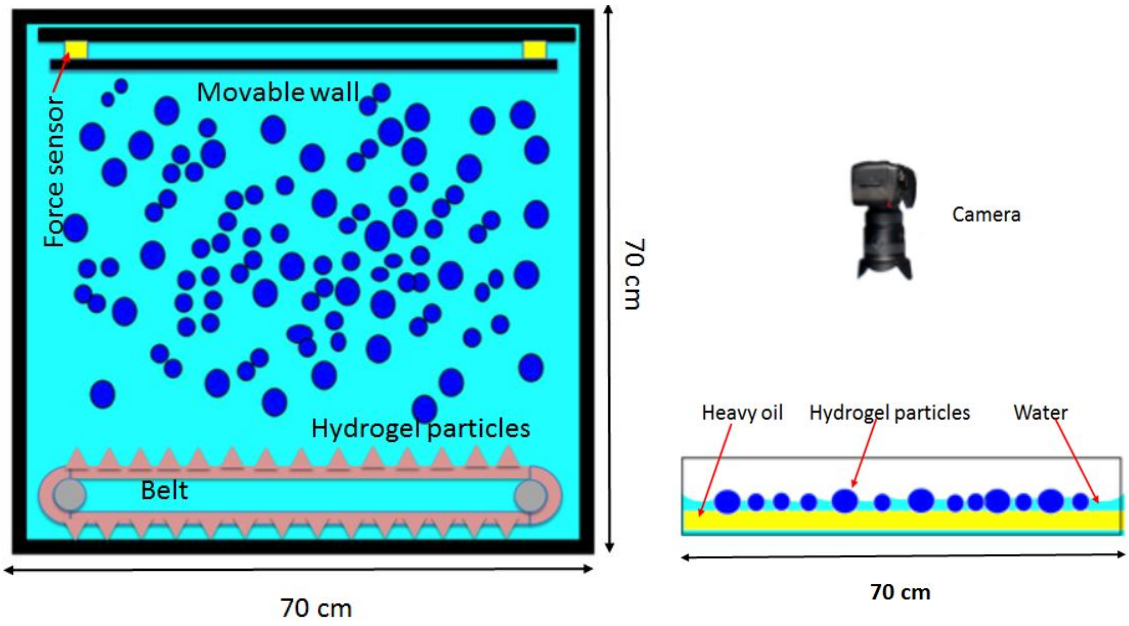

Fig.3 Diagram of the experimental setup. The image on the left is the view from the top: the pink part is the belt for applying shear, the blue spheres are the bi-dispersed hydrogel particles and the movable wall is on the back. The image on the right is a view from the side.

The experimental system is a two-dimensional, bidisperse, low-friction granular system that consists of 1000 - 1200 hydrogel spheres confined in a 70cm x 70cm x 5cm acrylic tank. The particles float on a layer of heavy oil and the packing fraction is controlled by a movable wall. One side of the tank is a belt that applies a shearing force to the particles. On the opposite side of the tank is a movable wall with sensors that measure the force inside the system. While shearing, the particles' movement are recorded by a camera, located about 1.5 m above the tank.

2.2 Granular system

The basic material of our hydrogel spheres is polyacrylamide. We bought the particles form JRM Chemical. In our system, we have 2 different sizes of particles, shown in Fig. 3. The small-to-large particle number ratio is 1:1, with small particles about 1 cm and large particles about 1.4 cm in diameter. Since we are interested in studying dynamic amorphous materials, we use a bidisperse system to avoid crystallization, which often occurs in monodisperse granular systems. The large sphere(dry) has a diameter about 0.3 cm and weighs about 0.022 grams and the small sphere is about 0.16 cm in diameter and weighs 0.008 grams. When placed in water, the large and small hydrogel spheres will absorb water and swell to diameters 1.4 cm and 1.0 cm, respectively. Because the volume increases dramatically when the spheres are put in water, the density of each hydrogel sphere is about 1.03 g/cm^3. The density of the fluorinert is about 1.94 g/cm^3, therefore, the fully swollen spheres will float on top of a 1 cm fluorinert oil layer.

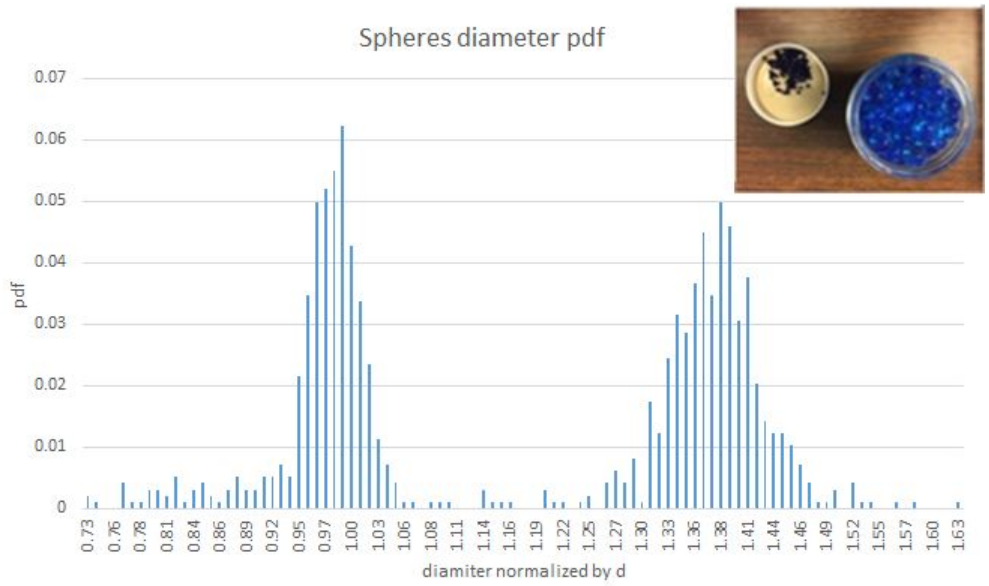

Fig.4 The distribution of particle diameters in our system. The inserted picture is the dried particles and swelled particles

The hydrogel is a very low-friction material [31-33]. The frictional coefficient for fully swelled spheres is about 0.01, which is very low compared to other experimentally studied grains. The gel-gel friction coefficient has been measured by Nicholas Cuccia in our lab. The coefficient is determined by the measuring the normal force and tangential force of a hydrogel sphere sliding on a hydrogel plane. The result is shown in Fig. 5. The shear velocity in our experiment is 0.5 cm/s, so the friction coefficient may be lower than 0.01.

The spheres float on a layer of FC-70 fluorinert (purchased from 3M corporation) to reduce the friction between the sphere layer and the bottom of the tank. The resulting drag force caused by the oil was small compared to the contact forces. The kinematic

viscosity of FC-70 is 12 cS (our experiments are conducted at room temperature) and the viscosity of water is approximately 1 cS.

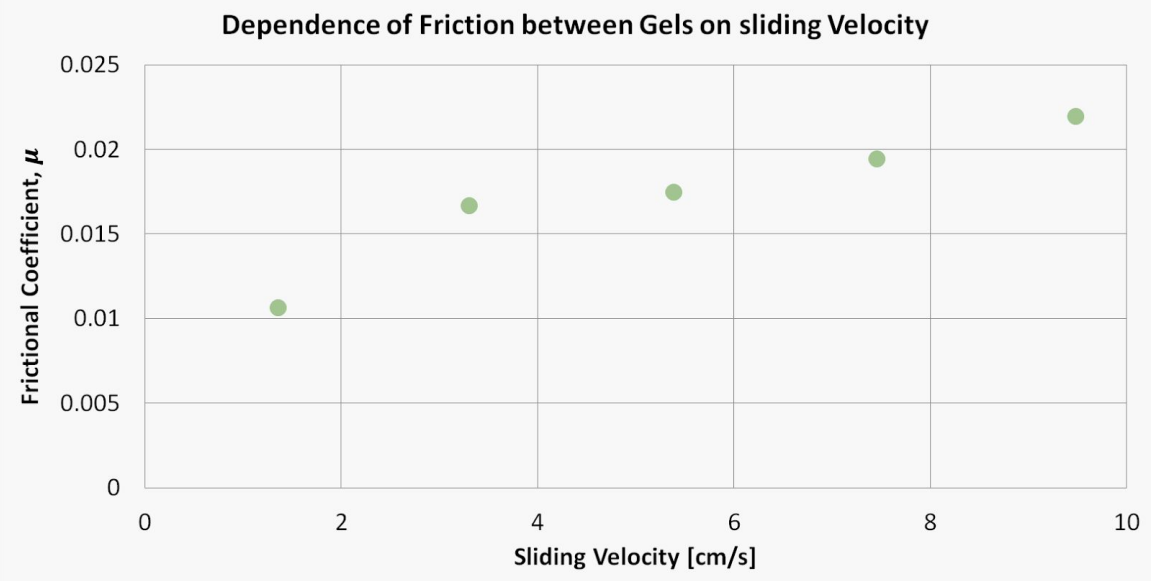

Fig.5 Measure of the frictional coefficient of the gel used in our experiment

2.3 Movable wall with force sensors

The packing fraction of the system, which we define as the area fraction viewed from above, was controlled by a movable wall. With a finite number of the hydrogel spheres in the tank, changing the position of the wall will change the packing fraction of the system.

2.3.1 Movable wall

The movable wall is a piece of 60 cm x 5 cm x 1 cm acrylic sheet, attached to a linear slider. A photo of it is shown in Fig. 6. The wall can be moved by the slider and the

wall spans the entire length of the system so that no spheres can fit behind the wall. One ruler is fixed on the top of the slider, so the movement of the wall can be measured with ~ 1 mm resolution.

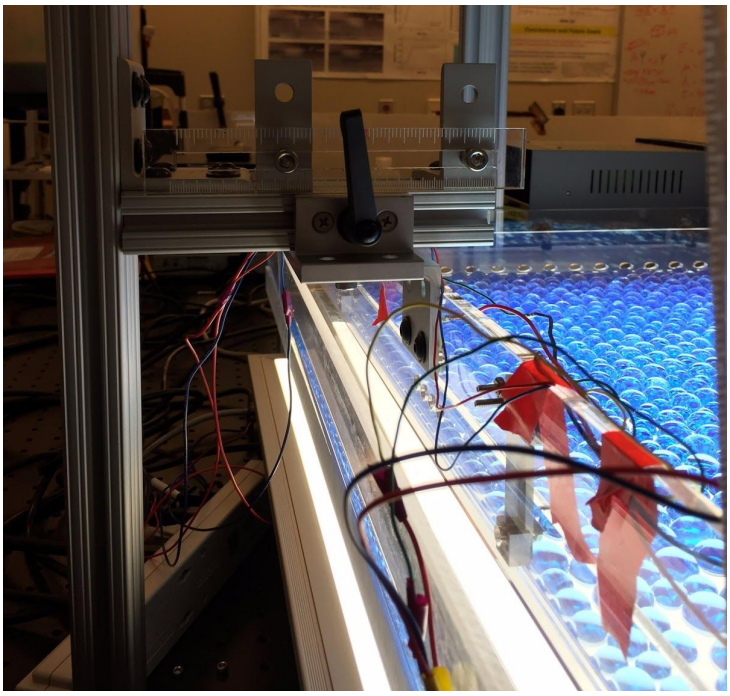

Fig.6 The photo of the movable wall attached to a slider and the two force sensors attached to the wall.

2.3.2 Force sensors

The two force sensors, purchased from Strain Measurement Devices Inc., were mounted on the movable wall. The max load for each sensor is 2 N and the suggested working voltage is 10V. The diagram of the force sensor and the corresponding circuit are shown in Fig. 7. When force is applied on the lower metal part of the sensor, the metal will deform. The sensor uses a thin-film strain gauge where the electrical resistance

changes according to the strain. In addition, a different working voltage will result in a different change in the output voltage, so for consistency, we always use the suggested voltage, which is 10 V.

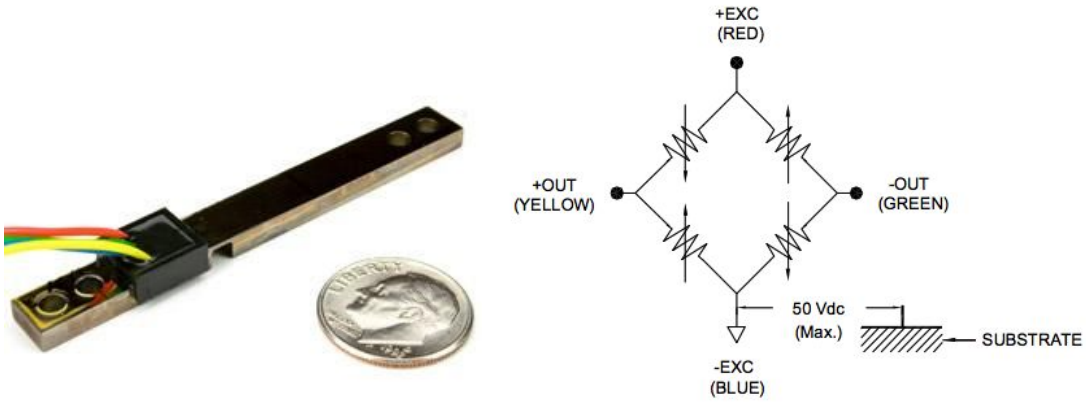

Fig.7 A photo of the sensor and a diagram of the force sensor circuit

On the movable wall we have two force sensors mounted evenly in order to avoid any torque caused by twisting. One small acrylic panel is attached on top of the two sensors, so the sum of the readout of the force sensors is the force applied to the acrylic panel. To calibrate the force sensors, we used a heavy pendulum touching the panel. By measuring the angle of the pendulum, we calculated the force on the panel, which is read by a data acquisition device through LabVIEW (National Instruments). We averaged the value over 500 seconds for calibration and the results are shown in Fig. 8. We tested forces in the range from 0.00 - 0.12 N. As we can see, the sum of the voltage varied linearly as the force increases on the panel.

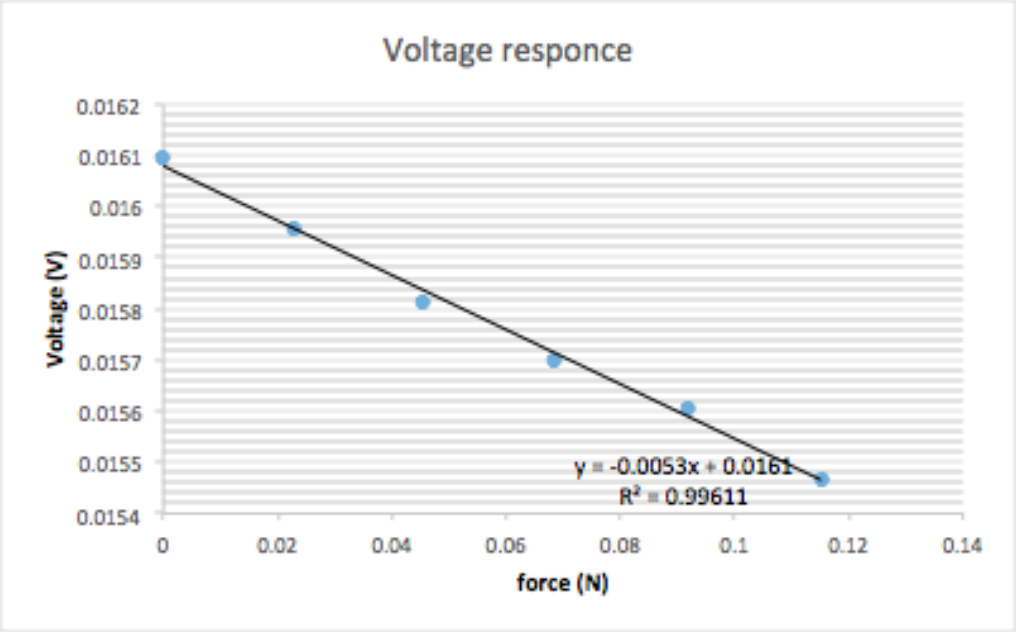

Fig. 8: The result of the force sensor calibration using a pendulum.

2.4 Shearing belt

The shearing belt is made of silicone rubber to prevent breaking of the particles. The belt design was made in AutoCAD and a mold was constructed to cast the silicone rubber (purchased from Zhermack Company). Because the friction between the particles and the silicon rubber belt is very low, we incorporated a belt with triangular teeth on the surface which prevents the particles from sliding along the belt. The interval of the teeth is about the same length as the diameter of the big particle and the length of the belt is about 50 cm. We used a laser cutter to cut an acrylic sheet into the desired belt shape and glued every part we cut together to make the mold. We then poured silicone rubber with the catalyst (1:1) into the mold with a plastic mesh inside and waited for 30 min for it to

solidify into a belt. The plastic mesh prevents the belt from twisting and stretching too much. The photos of our mold and a belt are shown in Fig.9. The motor for driving the belt is a compact square DC Gear Motor with a maximum torque of at 5.6 Nm at 1.2 rpm (24V). The speed and direction can be changed by the voltage and the polarity of current applied to the motor. For our experiments, we fixed the speed at 0.5 cm/s.

Fig. 9: The photos of the mold and the belt

Chapter 3

Data acquisition

There are two types of data we acquired during the experiment. The first one is the force data of the two force sensors; the other is the series of images recorded while shearing.

3.1 Force sensors' data

3.1.1 Force data acquisition system

The approximate pressure in the layer of particles was computed as the sum of the two force sensors. Each force sensor was connected to the analog side of an NI USB-6009, which is a data acquisition device which can measure the voltage and transmit the data to a computer (the system diagram is shown in Fig. 10). We used the differential mode to measure the force, which has the highest sensitivity and is isolated from ground. We used the Data Acquisition Assistant function in LabVIEW to acquire data from USB port and set the sampling rate for each channel to 24000 samples per second, which gave us a very fine resolution of data. We set the buffer size to 12000 samples, then averaged the samples together to minimize noise.

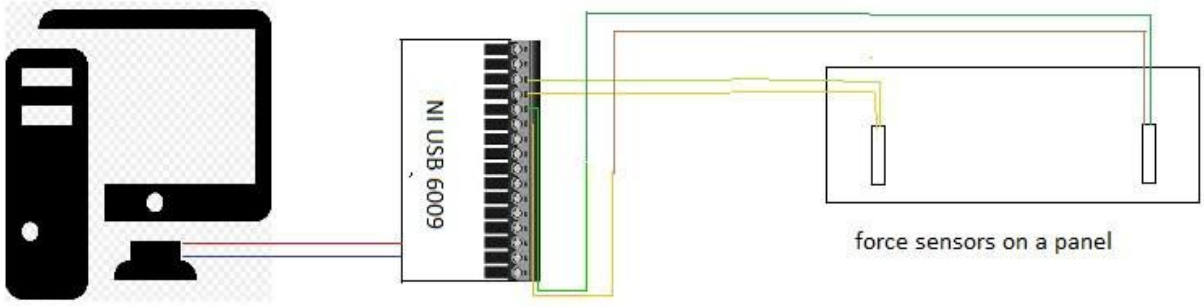

Fig.10: Diagram of the system to measure force

3.1.2 Relaxation of forces in the granular system

We changed the density of the 2D granular system by moving one side of the wall to increase confinement of the particles in the layer. One problem encountered was that when the system was very jammed, the system pressure took an extended period of time to relax after compression. Sometimes, the net force on the wall would gradually drop over a time scale of order 1000 seconds or greater. The sensors themselves have some inherent noise (about 0.002 N), so for all our measurements we waited until the decay in the force was less than the amplitude of typical fluctuations. After compression, if the dynamic average over 100 seconds changed less than 0.002 N, we assumed the system was stable and we commenced our measurement. Fig. 11 is the total force data after compression and before shearing. The compression first drastically increase the force, and then the force then relaxed, and at about 700 seconds in the data, we consider the relaxation to be sufficient. We then recorded the total force for 100 seconds without shearing, then started shearing at a speed of 0.5 cm/s. We recorded the total force and

simultaneously imaged the entire system from above for 1000 seconds.

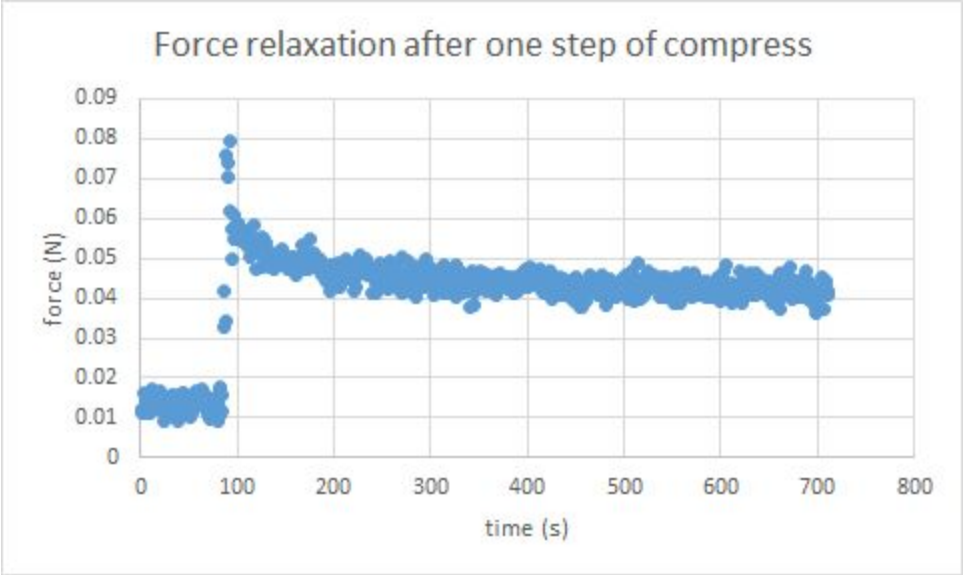

Fig.11: The force sensors' data rise after pushing the moving wall forward. The total force experiences a relaxation phase prior to the beginning of the shear.

3.1.3 Choosing the valid data and adjust threshold

When the system begins to jam, the total force experienced a sharp increase. Fig. 12a shows the force data for different densities. For very dense packing fractions when the system was compressed too much (the contact force between adjacent spheres was large), spheres would "pop out" of the quasi-2D layer due to a buckling instability (see Fig. 13). This buckling instability released in-plane stress and thus caused a decrease in the net force. This affected the pixel density measurement, which is one method by which we characterize the system packing fraction. This can be seen in Fig. 13, which is the 7th data point of Fig. 12a. There are some spheres popping out of the plane. A zoomed-in

image of the popped-out sphere is shown in Fig. 13b. The force for holding one particle on the top of the particle layer can be estimated using the amount of work necessary to lift a neutrally buoyant object out of a fluid. The work necessary to lift one particle is $W = m\,g\,d_0/2$, where m is the mass of the particle and g is the acceleration due to gravity. The factor of 1/2 is due to the average force as the particle is lifted out of a neutrally buoyant state. Popping a single particle out of the layer changes the density by $\sim 1/N$, where $N \sim$ 1200 particles. This work is equated to the total force on the wall F multiplied by L/N, where L is the length of the system (~ 70 cm). The necessary wall force is then $F \sim 0.1$ N, which is just slightly larger than the threshold we measure. This will also affect the measurement of force since the strain is reduced when particles pop out (Fig. 12a). In addition, this will also reduce the density from our image analysis. Because all these problems, we will only consider data for experiments below the buckling threshold.

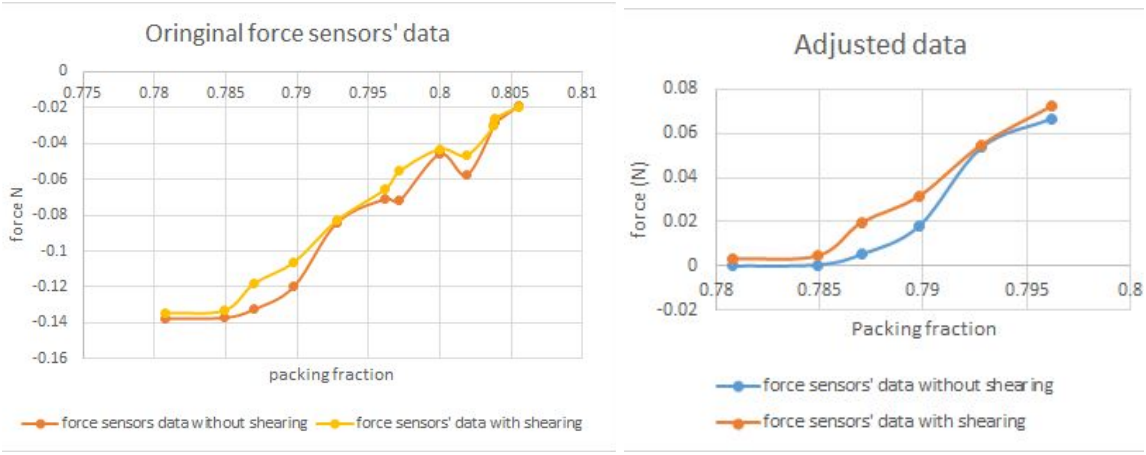

(a) (b)

Fig. 12: (a) Original data of shear force and baseline force. (b) Adjusted shear force and baseline force data for systems where spheres remain in the quasi-2d layer.

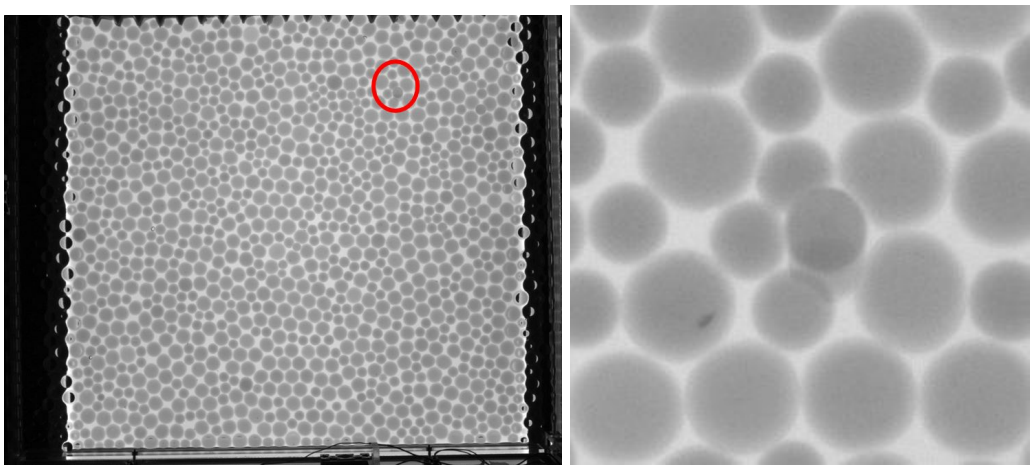

(a) (b)

Fig. 13: (a) A picture of the system while shearing. This corresponds to the 7th data point for the shear force. (b) A zoomed-in picture for (a) at a small region with a sphere popping out of the plane.

Another adjustment we should make is an adjustment of the zero point. The coefficient of the voltage-force response has already been calibrated (Chapter 2.3.2). However, we found that the threshold may sometimes change according to water level or number of particles attached to the panel. So, for all the data we use the average force in the low packing fraction system (unjammed) without using the shearing as the zero point, and then subtract this from subsequent data (adjusted data is plotted in Fig. 12b.

3.2 Image analysis

We used a PointGrey monochrome camera with a Sony ICX814 (resolution 3380x2704 pixels) sensor and a wide angle lens. The images were recorded during the shearing over 1000 seconds at a frame rate of 1 frame per second.

3.2.1 Determination of system packing fraction

In order to measure the packing fraction of the system, we first turned the grayscale images into binary images, which only have black and white pixels shown in Fig. 14. Then, we calculated the percentage of black pixels in the system as a measurement of the packing fraction. However, the value of the pixels is distributed in range 0 - 255 in a grayscale image, so we needed to set a threshold value to determine which pixel is white and which is black. The choice of the threshold can greatly affect the value of the packing fraction. If we choose a threshold that is too large, the shadows of spheres near the edges will be counted as parts of spheres, and if we choose a value that is too small some areas on the edges of spheres will be cut off. For consistency, we always used the same threshold for binarizing every image. Even though we cannot get the exact packing fraction value from this method due to systematic errors, we obtained to relative difference between packing fraction and the critical packing fraction.

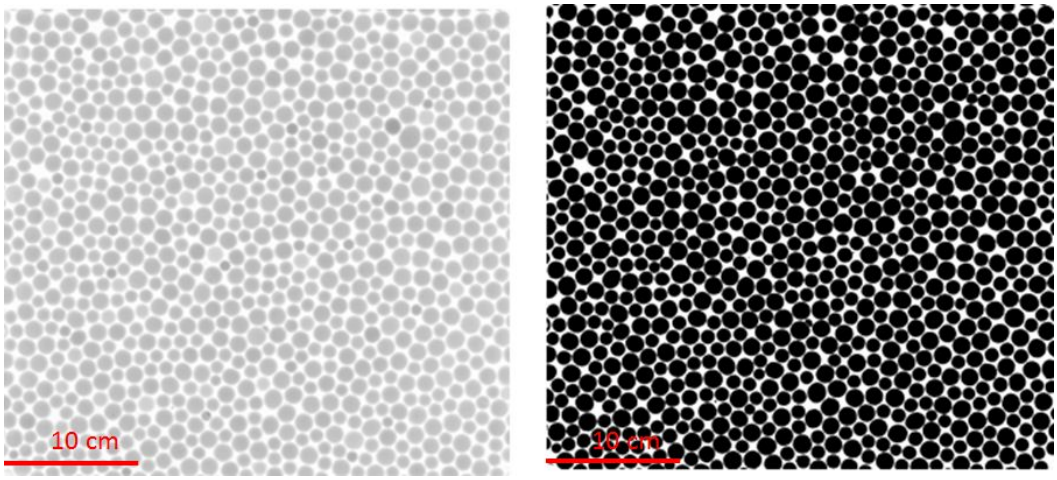

Fig.14: a typical grayscale image from the experiment and the corresponding binary image.

We used the data from the force sensors to determine the point at which the system is jammed which determined our measurement of ϕ_c from the image analysis. We tested the relationship between the system pressure and the packing fraction by using the movable wall; each compression moved the tank inwards 0.32 cm, which applied a uniaxial compression to the system. The pixel density linearly increases as the compression distance increases from 0 cm to approximately 1.5 cm as shown in Fig. 15a. This further confirms that it is reasonable to use pixel density to determine the density difference between two packings. We see that after a particular value of the compression, the force response increases dramatically compared to preceding that point (for both types of force data, with and without shearing). We can use the kink of the force data to determine the jamming point ϕ_c .

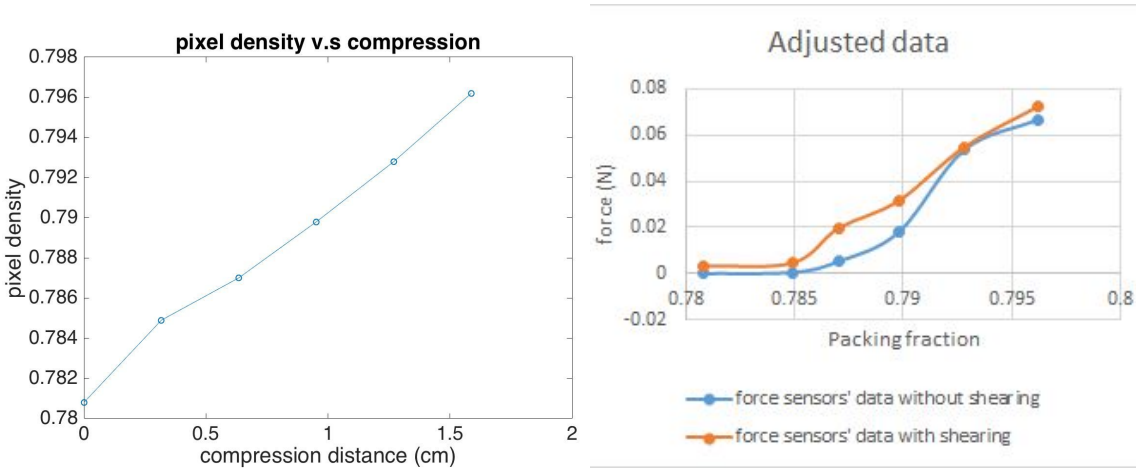

(a) (b)

Fig. 15 (a) Pixel density vs. compression distance. (b) Change in the force on the movable wall in response to compression to the movement of the wall (same as Fig. 12b).

3.2.2 Particle tracking

We used Trackpy [34] (an open source Python tracking software) to track the spheres. After detecting the spheres' center for each frame, the software gave an identification number to each sphere and then linked the particles' position from frame to frame in order to get the trajectories. The speed of the shear was 0.5 cm/s, so the speed of the spheres will not exceed 25 pixel per second. We used 20 pixels as a search range (the maximum distance away from the original particle position to find the same particle in next frame) in our analysis to optimize computational time.

Some of the particles' tracks were lost near the boundaries. This may be due to: 1) some particles going too fast (which usually happens near the shearing belt) such that the position is larger than the tracking threshold, or 2) the cropping of our images on the edges of the experimental setup. If, during recording, the particles move in and out of the cropping zone, the tracking information will be not continuous, meaning that the tracking algorithm will interpret this as more than one particle's track, resulting in a false detection. Because of this, we filtered the tracks shorter than 100 seconds, which eliminated some of the particles' tracks in the corners.

Chapter 4

Experimental results and analysis

4.1 Results of force measurement

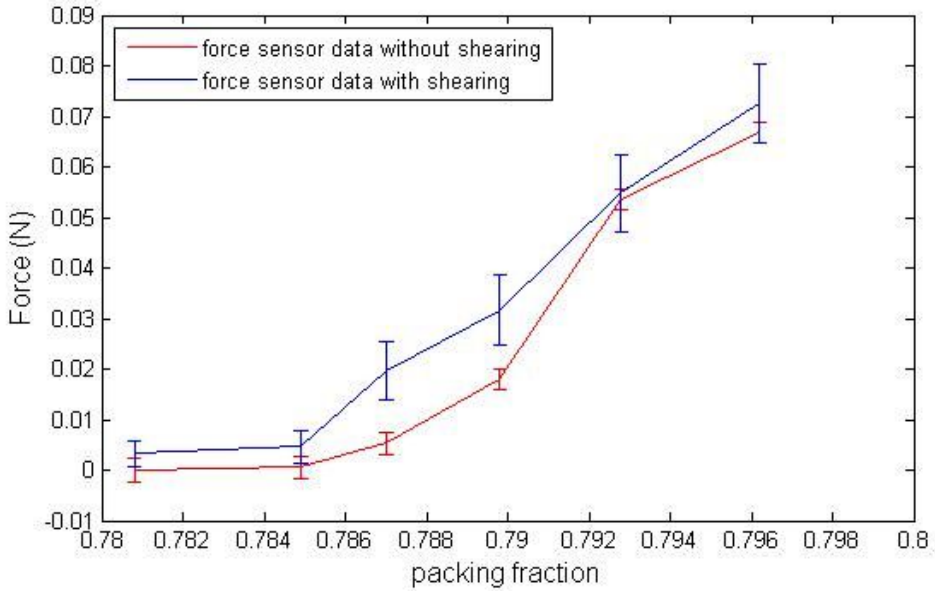

Fig. 16: Force sensors' data with and without shearing for six different packing systems (same data as shown in Fig. 12b and Fig. 15b)

In order to determine the jamming point we first used the force sensors' data vs. the pixel density, shown in Fig.16. For both lines (with or without shearing). The trend before $\varphi = 0.785$ (the second data point from left) is flatter than the trend after $\varphi = 0.785$. Previous jamming studies have shown that the system pressure will increase as the system transitions from the unjammed to jammed state, so according to our data, the

jamming point is probably between the 2nd and 3rd data point.

We also see a separation between the force data with shearing and without shearing. This is likely caused by the natural dilatancy of granular materials, which is a tendency for granular materials to dilate while shearing. As the material expands, the pressure in the system, and thus the force on the wall, will increase since the system is confined. We also see that after the jamming point, the data for the unsheared and sheared systems are significantly different, as shearing the system has a large effect on the pressure. Then, this difference between the data becomes smaller at higher packing fractions. The closing of the gap is correlated with the saturation of the growing length scale at the system size, which will be discussed in section 4.6.

4.2 Analysis of density in y-direction

One important question concerns inhomogeneity in the density of the system. Near the shearing belt there could be more dilation due to the constant particle rearrangements. Fig.17 is pixel density in the y-direction averaged over time for the six systems corresponding to the six force sensors' data. The data was averaged over all the frames in a given experiment in order to reduce noise and look for persistent deviations from uniform density. At low density, we can see some clear variations in the density, which is because the spheres have very little movement. However, after the packing fraction increases, there is less variation in the data. This is because the increase in movements of the spheres will smooth out the structure after averaging over many

frames.

By looking at the general trend for each graph, we can also see in the low-packing fraction system, the local density near the shear zone is slightly lower than the average of the whole system. In addition, this also corresponds to the closing of the gap between the force sensors' data with and without shearing. The relationship between the system pressure (wall force) and the local density variations is unclear, and requires further experimental investigation.

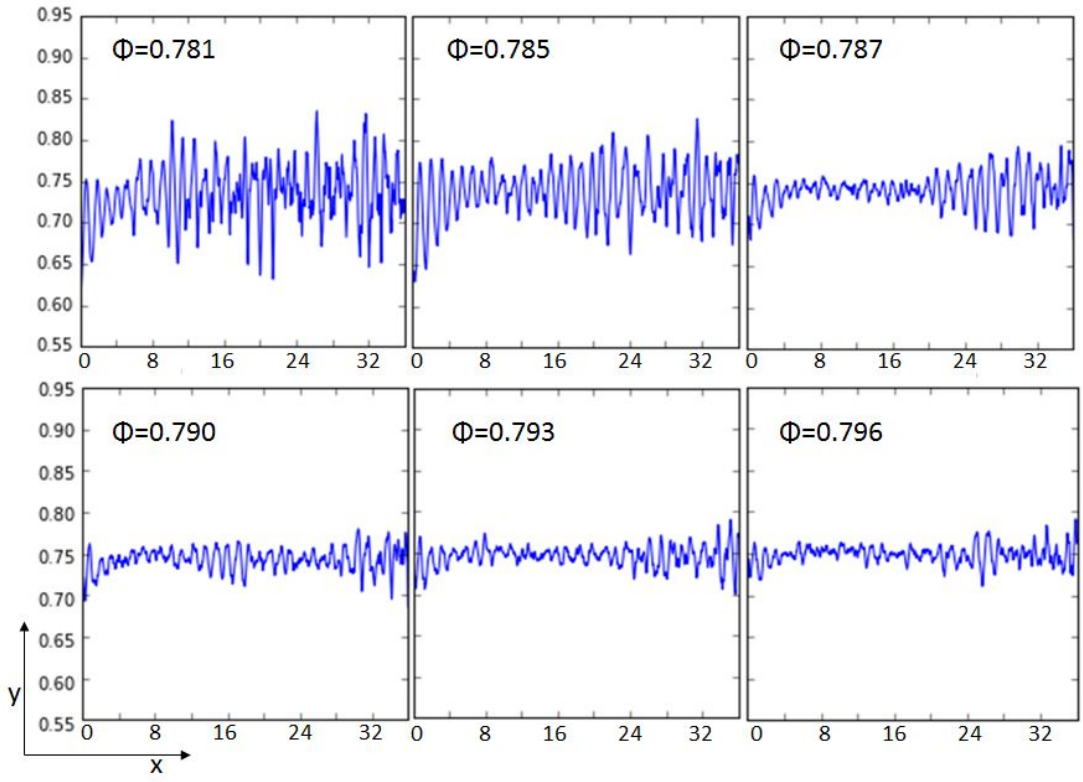

Fig.17 The averaged pixel density changing in y direction (normalized by d_0 average particle diameter) in six different packing fractions over 1000 seconds

4.3 Particles' trajectories

A close inspection of the dynamics of the particles during shear reveals intermittent, collective motion consistent with a growing length scale. We took 1000 images at a frame rate of 1 frame per second in six different systems of different density, simultaneously with the force measurement, so the six data points of force correspond to the six sets of images.

The tracks shown in Fig. 18 are from the six different packing fractions $\Delta\phi$ ($\Delta\phi = \phi - \phi_c, \phi_c = 0.785$) varying from -0.004 to 0.011, and each track represents 200 seconds of data (only 200s were shown here for clarity). For systems with a packing fraction greater than 0.796 ($\Delta\phi = 0.011$), we experimentally observed spheres popping out of plane. Below $\Delta\phi = -0.004$, we cannot clearly see the motion of the spheres because the system is unjammed. Starting from $\Delta\phi = 0$ (the second set of data) to $\Delta\phi = 0.008$ (the fifth set of data), we see a region near the shearing belt that has larger movement than the spheres in far away from the shearing belt. The size of this region seems to grow gradually as the packing fraction increases.

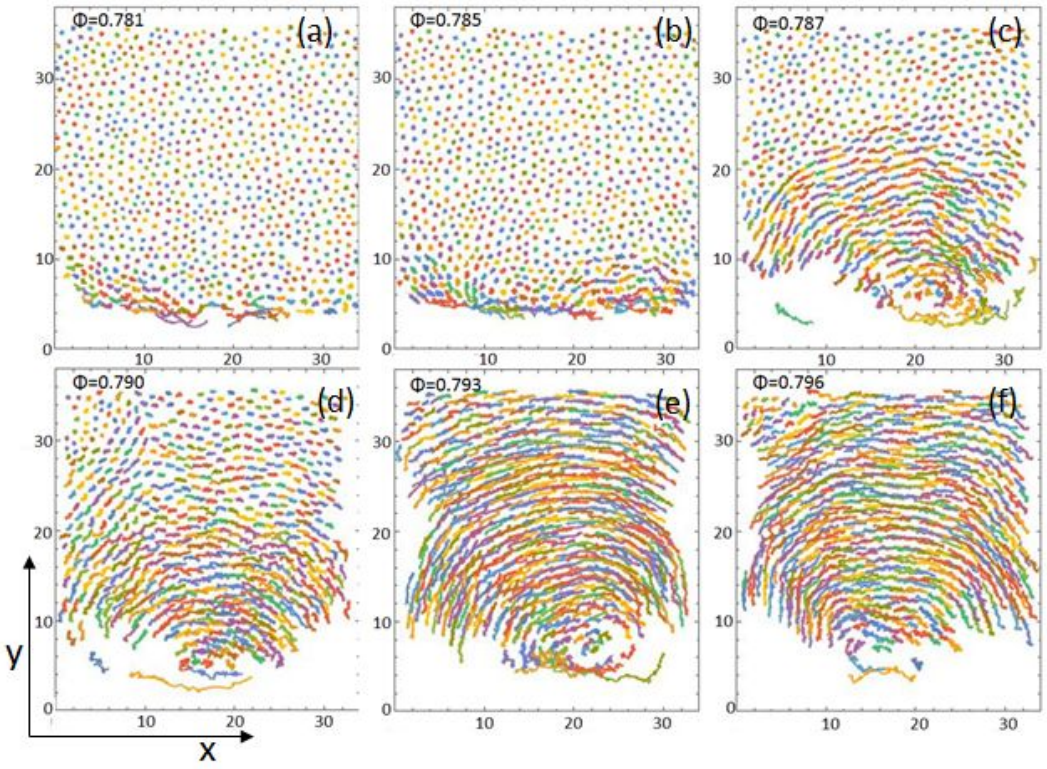

Fig. 18: Trajectories of spheres in systems with six different density over 200 seconds start from t = 100 s. The packing fraction for the six data set are (a) $\varphi = 0.781$, (b) $\varphi = 0.785$, (c) $\varphi = 0.787$, (d) $\varphi = 0.790$, (e) $\varphi = 0.793$, (f) $\varphi = 0.796$. The x and y axis are normalized by averaged particle diameter d_0 .

4.4 Displacement distribution

A visual inspection of Fig.18 indicates that there is a clear growth of particle motion far from the shear belt as the system becomes denser. Next, we tried to determine a method of quantifying this trend. We looked at the distribution of the displacement of each sphere. From Fig.19a to Fig.19f, there are the six data sets corresponding to the six trajectory graphs in Fig.18. The displacements were normalized by the averaged particle diameter d_0 . In Fig. 19a, the majority of the particles barely move, so we see a very sharp

peak at displacement equal $0.5\,d_0$. In graph Fig. 19b, the position of the peak shifts to about $1.5\,d_0$, and in Fig. 19c the peak shifts to $3.5\,d_0$, and in Fig. 19d at $5\,d_0$. We also see the median value of the distribution shift to the right, meaning that the majority of particles in the system move faster with an increasing packing fraction. In Fig. 19c, we start to see there are two peaks in the distribution. This is because the spheres near the shear zone have more motion than the rest of system. We can see a very clear boundary separating a rigid, rotating cluster, and a group of spheres near the top corners of the system. This separation is most clear in Fig. 18c. As the system becomes denser, this boundary become more indistinguishable, although there still exists a bimodal distribution.

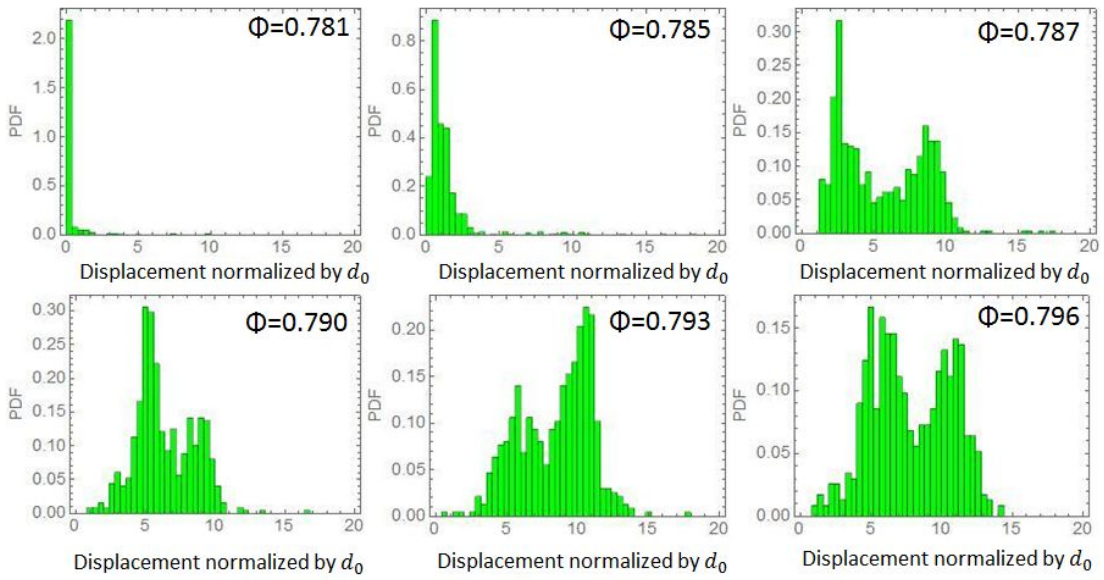

Fig. 19: distribution of the displacement over 1000 seconds of systems with six different packing fractions.

4.5 Decay of velocity away from the shear zone

We also analyzed the relation between the average particle velocity and distance from the shear zone. We divided the images into rectangles 50 pixels in height in the y-direction, then averaged the particle displacement within each rectangle over the whole video. In Fig. 20, we observe that after an initially sharp drop, the low density system shows significant decay in the y-direction, and high density systems have very little decay. This is very similar with results observed by the other shearing granular materials experiments [36-39] where the velocity decays much more rapidly from the shear zone.

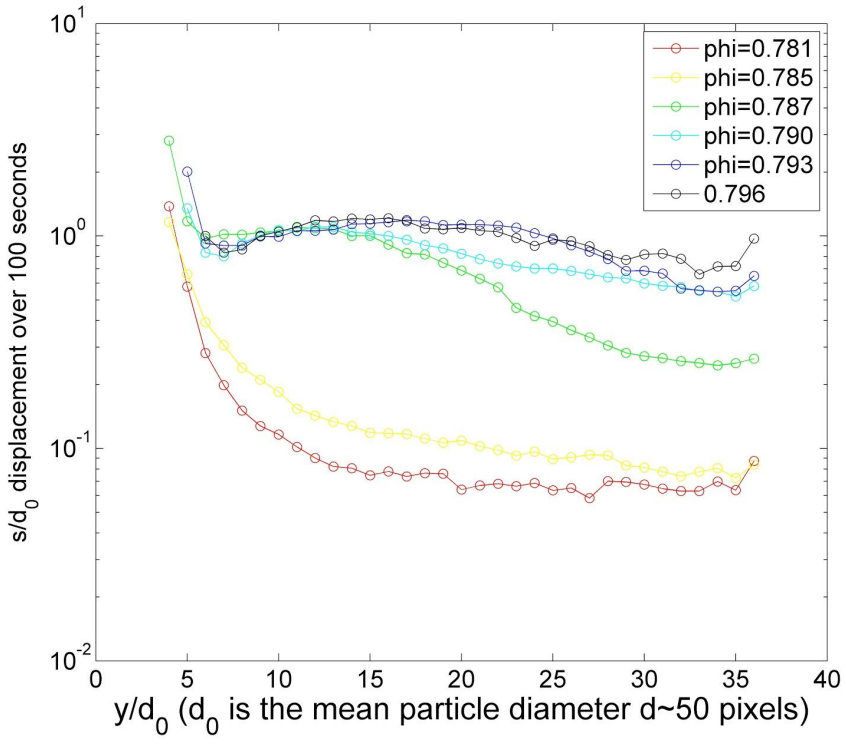

Fig. 20: Average displacement for 100 seconds vs. distance from the shearing belt, *y,* normalized by mean particle diameter.

4.6 Analysis of moving particle clusters

In order to look further at how the particles' movements are correlated, we plotted the displacement fields. We chose the time at t = 500 s, and calculated the displacement corresponding to $\Delta t = 100\ s$. The displacement field of packing fraction 0.787 and 0.793 is show below in Fig. 21. We can see that there is a group of particles behaving like a rotating rigid body. The rigid body behavior is excited by the shear and its size changes according to the packing fraction.

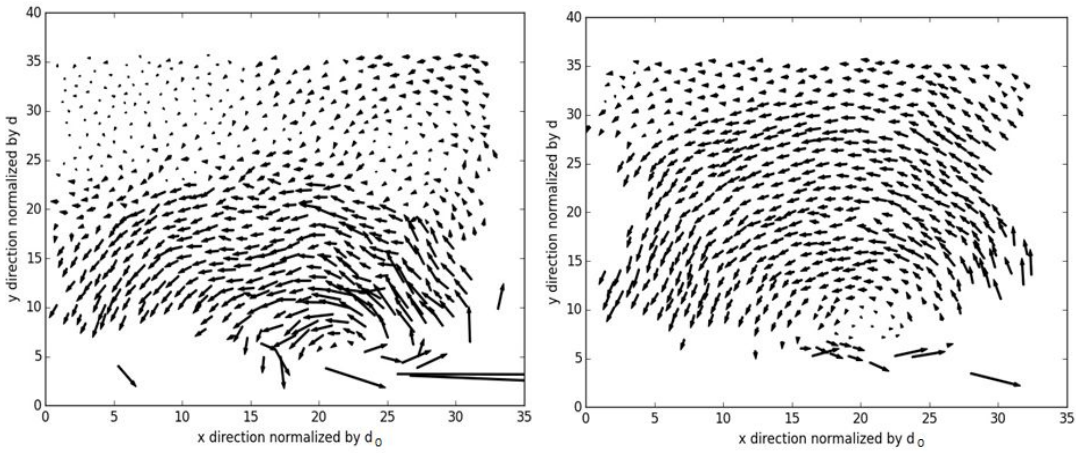

(a) (b)

Fig. 21: Particle displacement field over 100 seconds for systems with density (a) 0.787 (compression 6.35mm, third data point with shearing) and (b) 0.793 (compression 12.7mm, the fifth data point with shearing)

To quantify this shear-induced rigid body behavior, we define a cluster of spheres which has more movements than others. The way we defined the cluster is by choosing a threshold for displacement so that if a sphere has displacement larger than the threshold, we then count it in the cluster. We used the center of the cluster to quantify the size of the

cluster. We tried different threshold values: $0.5\,d_0$, $1\,d_0$, $1.5\,d_0$, $2\,d_0$, $2.5\,d_0$ and $3\,d_0$. The result of the analysis is plotted in Fig. 22a-b.

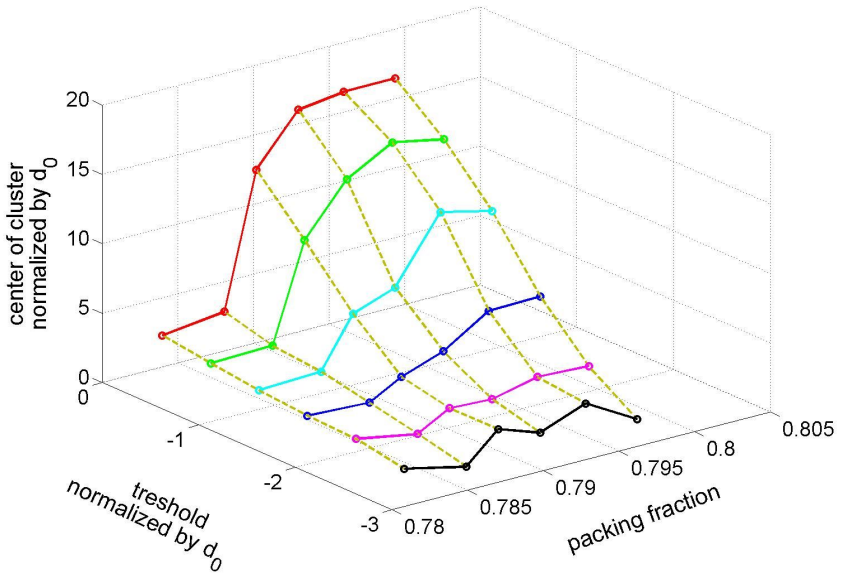

(a)

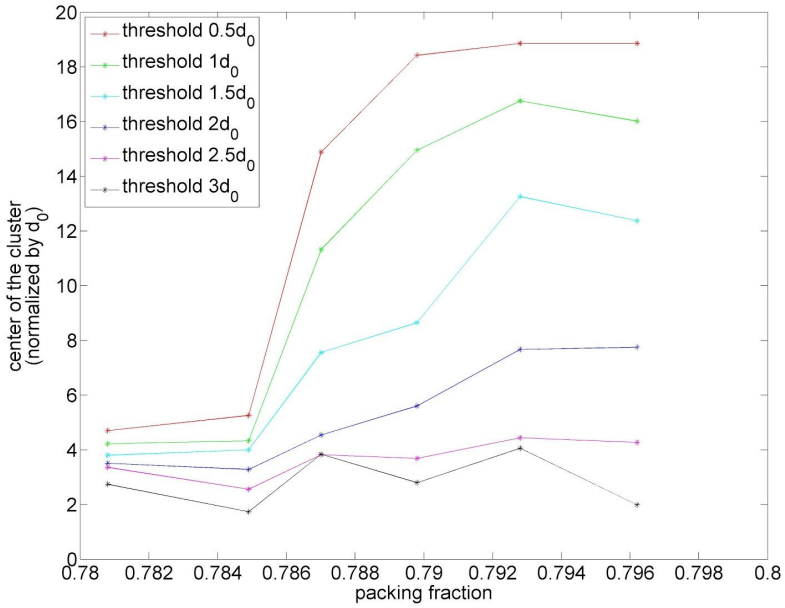

(b)

Fig. 22: (a) The center of the defined particle cluster with different thresholds and packing fractions (b) Projection of (a) onto the packing fraction and center position plane.

No matter which threshold we choose, the trend is very clear: the cluster size has the largest jump at 0.785, which is the jamming point. However, the cluster size continues to grow after the jamming point and reaches a plateau at packing fraction of about 0.793. This may imply that even though the force chains percolate throughout the jammed system in all directions, it may not be enough to form a collective movement of particles over the entire system during shearing. This behavior is a bit contradictory to our previous expectation of behavior near jamming. The experiment and simulation results in static systems show that the characteristic length scale diverges at the jamming point, which means that the particles in the whole system are correlated with each other. This may lead one to intuitively think that in a dynamic system, particles move collectively as a whole body at the jamming point and that the size of the collective, rigid body movement may have a maximum at jamming point. However, this is not what we observed in our experiment.

Chapter 5

Conclusion, discussion, and future direction

5.1 Conclusion and discussion

In our experiment, we built a quasi-2d, low friction granular system. We used force sensors to determine critical value of density and used image analysis to measure the density and track the motion of the particles. We continuously applied shear to the system and we found the particles move in response to the shear, but that the movement depends sensitively on the density. The motion has a sharp increase at jamming point and the extent of the particles' motion grows until it reaches the system size at a packing fraction which is larger than the packing fraction at which the system begins to jam.

This may contradict our previous hypothesis that the jamming point is a point at which the cluster size of rigid body movement should have reached a peak because many well-known length scales in jammed systems diverge at the jamming point, however, this is not what we observed. Interestingly, we observed the length scale growing and reaching a maximum at a little higher than the critical packing fraction. This growing length scale may suggest that there are some intermittent states near jamming point. This speculation is supported observed by Dapeng Bi et al. [27], where the authors presented a phase diagram with these intermittent states in a "shear jamming" region near the

jamming point. However, the extent of the shear jamming region has yet to be fully explored. We speculated that in our experiment there may be a packing fraction φ_x in which these intermittent states disappear. An adapted version of the phase diagram which conveys this idea is shown in Fig. 23.

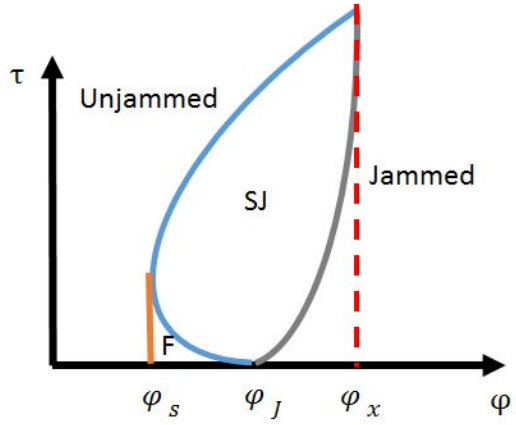

Fig.23: An alternative version of jamming diagram with intermittent states and with an indication of position of the φ_x. SJ is the shear jamming state and F is the fragile state discover by Dapeng Bi et al. [27]. φ_J is the jamming point; φ_s is the shear jamming point.

In addition, the length scale behavior in our experiment doesn't diverge at a specific packing fraction and instead it gradually flattens out. This may due to finite-size effects in our experimental environment. Similar effects are also observed in some very recent simulations in which significant differences were observed in frictionless systems prepared by shear and compression [40]. This difference was decreased for larger systems, and scales as $1/N^{1/2}$. This possible explanation would require further experiments with different system sizes, but our experiment still highlight the difference between static jamming and dynamics in sheared granular systems.

5.2 Future direction

To extend this work, future experiments could be done with a finer control of the packing fraction, especially when this rigid cluster first begins to grow. This can be achieved by adjusting the movable wall with finer steps. Another improvement for our experiment could be using a sensitive current meter to measure the torque on the motor, and thus the overall shear force on the system.

In addition, to further investigate this growing length scale near the jamming point, we can look what φ_x depends on, such as different system sizes or the ratio of width and length of the system. Currently, we are using a 1:1 width and length ratio, but we can vary this by adding a movable side wall. Alternatively, we could use a tank with different geometry, like a cylinder, which would allow for a more symmetric shearing geometry without side walls.

References

[I] C. A. Coulomb, Acad. R. Sci. Mem. Math. Phys. par Divers Savants 7, 343 (1773).

[2] O. Reynolds, Philos. Mag. 20, 469 (1885).

[3] R. A. Bagnold, Proc. Roy. Soc. London A 225, 49 (1954)

[4] C. S. Campbell, Annu. Rev. Fluid Mech. 22, 57 (1990).

[5] A. J. Liu and S. R. Nagel, Nat. Phys. 396, 21 (1998).

[6] C. S. O'Hern, L. E. Silbert, A. J. Liu, and S. R. Nagel, Phys. Rev. E.68, 011306 (2003).

[7] C. S. O'Hern, S. A. Langer, A. J. Liu, and S. R. Nagel, Phys. Rev. Lett. 88,7 (2002)

[8] G. Biroli, Nat. Phys. 3, 222-223 (2007)

[9] P. Olsson and S. Teitel, Phys. Rev. Lett. 99, 178001 (2007).

[10] M. Wyart, S. R. Nagel and T. A. Witten, Europhys. Lett. 72, 3 (2005)

[11]C. P. Goodrich, W. G. Ellenbroek, and A. J. Liu, Soft Matter 9, 10993-10999 (2013).

[12] S. S. Schoenholz, C. P. Goodrich, O. Kogan, A. J. Liu and S. R. Nagel, Soft matter, 9, 11000-11006 (2013).

[13] C. Heussinger and J. L. Barrat, Phys. Rev. Lett. 102, 218303 (2009).

[14] M van Hecke, J. Phys. Condens. Matter 22, 033101 (2010)

[15] L. E. Silbert, A. J. Liu, and S. R. Nagel, Phys. Rev. Lett. 95, 098301 (2005)

[16] W. G. Ellenbroek, E. Somfai, M. van Hecke, and W. van Saarloos, Phys. Rev. Lett.

97, 258001 (2006)

[17] S. Alexander, Phys. Rep., 296, 65 (1998).

[18] M. C. Fernando, Phys Rev. Lett. 81,8 (1998)

[19] M. Wyart, Ann Phys. 30, 3 (2005)

[20] D. J. Durian, Phys Rev. Lett. 75, 26 (1995)

[21] X. Cheng, Phys. Rev. E, 81, 031301 (2010)

[22] P. C. Johnson and R. Jackson, J. Fluid Mech. 176, 67 (1987).

[23] H. M. Jaeger, C. Liu, S. R. Nagel, and T. A. Witten, Euro. phys. Lett. 11, 619 (1990).

[24] T.G. Drake, J. Geophys. Res. 95, 8681 (1990)

[25] D. M. Hanes and D. L. Inman, J. Fluid Mech. 150, 357 (1985).

[26] K. To, P. Lai, and H. K. Pak, Phys. Rev. Lett. 86, 1 (2001)

[27] D. Bi, J. Zhang, B. Chakraborty, and R. P. Behringer, Nature 480, 355-358 (2011).

[28] H. Zheng, J.A. Dijksman and R.P. Behringer, Europhys. Lett. 107, 3 (2014)

[29] A. J. Liu and S. R. Nagel, Annu. Rev. Condens. Matter Phys. 1, 347-369 (2010).

[30] M. Otsuki and H. Hayakawa, Phys. Rev. E. 83, 051301 (2011)

[31] L. P. Kadanoff, Rev. Mod. Phys. 71, 435 (1999).

[32] H. Y. Ren, M. Mizukami, T. Tanabe, H. Furukawa, and K. Kurihara, Soft Matter, 11, 6192–6200 (2015).

[33] B. Andreotti, F. Yoël, and O. Pouliquen, Granular Media: between Fluid and Solid,

Cambridge University Press, New York (2013)

[34] http://soft-matter.github.io/trackpy/v0.3.2/

[35] B. Andreotti, Y. Forterre, and O. Pouliquen, Granular Media: between Fluid and Solid, Cambridge University Press, 2013

[36] O. Pouliquen and R. Gutfraind, Phys. Rev. E 53, 1 (1996).

[37] D. Howell, R. P. Behringer, and C. Veje, Phys. Rev. Lett. 82, 26 (1999).

[38] T. S. Komatsu, S. Inagaki, N. Nakagawa, and S. Nasuno, Phys. Rev. Lett. 86, 9 (2001).

[39] G. Debrégeas,H. Tabuteau, and J.-M di Meglio, Phys. Rev. Lett. 87, 7 (2001).

[40] M. Baity-Jesi, C. P. Goodrich, A. J. Liu, S. R. Nagel, and J. P. Sethna, cond-mat.soft arXiv:1609.00280 (2016)